Ceramics International 47 (2021) 17041–17048

Contents lists available at ScienceDirect

Ceramics International

journal homepage: www.elsevier.com/locate/ceramint

$CaO–MgO–SiO_2–P_2O_5$- based multiphase bio-ceramics fabricated by directional solidification: Microstructure features and in vitro bioactivity studies

María Díaz-Pérez [a], Lorena Grima [a], Bibi Malmal Moshtaghioun [a,b], José Ignacio Peña [a,*]

[a] Instituto de Nanociencia y Materiales de Aragón, CSIC-Universidad de Zaragoza, 50009, Zaragoza, Spain
[b] Departamento de Física de la Materia Condensada, Universidad de Sevilla, PO Box 1065, 41080, Sevilla, Spain

ARTICLE INFO

Keywords:
Ceramic scaffolds
Monticellite
Akermanite
Tricalcium phosphate
Nurse's A phase
Laser floating zone

ABSTRACT

In vitro activity is important when considering the choice of a multiphasic bioceramic scaffold as phases can dissolve or transform at different rates. The aim of this study is focused on the synthesis and in vitro analysis of multiphasic ceramics obtained from the melt by directional solidification. Depending on the growth rate of the new composition different bioactive phases coexist in the same sample: akermanite, monticellite, tricalcium phosphate and Nurse's A phase, all of them with potential in the medical area as implant for bone or dental repair. With the knowledge of what and how phases dissolve first, it was possible to design materials to get porous scaffolds or more stable ceramics.

1. Introduction

During the last decades, due to the increase in the age of the population, there is a greater incidence of musculoskeletal pathologies (fractures, osteoporosis, bone infection or tumours). Autografts, allografts and xenografts are the most used therapies but can carry some limitations like graft rejection problems, limited sources of bone or transmission of diseases.

Tissue engineering can help to solve these limitations through the development of porous matrices (scaffolds) that provide structural and mechanical support to cells for their attachment and proliferation. Main scaffold requirement is to present similar properties to the tissue where implanted. In particular, the material used as a bone substitute must meet the following demands: non-toxicity, biocompatibility, osteoreproductivity and osteoconductivity, be bio-absorbable and have adequate mechanical properties to provide a structural support during bone growth and re-modelling [1].

One type of bioactive material is surface active silicate-based ceramic that can generate hydroxyapatite (70% of the composition of the bone) in contact with Simulated Body Fluid (SBF), a solution with an ionic concentration, pH and physiological temperature close to that of human plasma, which can also provide mechanical support to cells. It is known that wollastonite, akermanite, monticellite and forsterite meet these specifications.

Akermanite is a silicate bioceramic widely used in clinical applications due its excellent properties in bone regeneration. Y. Huang et al. [2] used akermanite and nagelschmidtite to investigate the inflammation responses in vitro and in vivo to increase the understanding on the osteogenic activity of this ceramics and provide guidance to design new bioceramics with potential applications in bone tissue engineering. They found that both ceramics compared with TCP, a remarkable bone repairing bioceramic, significantly decreased the immune responses caused by macrophages influenced by Mg, Ca an Si ions released in adequate concentrations.

The bioactivity of monticellite was studied by Chen et al. and Kalantari et al. [3,4]. They demonstrated that an apatite-like layer was formed on the surface of SBF-soaked monticellite samples after 14 days. Moreover, in vitro evaluations showed that monticellite is biocompatible over mouse osteoblast-like cells (G292).

Both, TCP and Nurse's A phase are known for their strong bioactivity. TCP ceramics are widely used in bone tissue regeneration because of their good biocompatibility, similar chemical composition with biological apatite and osteoconductivity properties [5–7].

The biological activity and material properties of Ca–P scaffolds improve with the presence of Si, as this element plays an important role in the development of healthy bone and connective tissues [8]. The in

* Corresponding author.
E-mail address: jipena@unizar.es (J.I. Peña).

https://doi.org/10.1016/j.ceramint.2021.03.011
Received 22 December 2020; Received in revised form 1 March 2021; Accepted 2 March 2021
Available online 5 March 2021

vitro behaviour of the Nurse's A phase as scaffolds for bone tissue engineering applications has been studied by R. Rabadan-Ros et al. [9].

Forsterite has superior mechanical properties compared to others bioceramics and glasses, possesses slow HA deposition ability and stimulates proliferation and adhesion of osteoblast cells [10]. Choudhary et al. [11] demonstrated the potential of this ceramic potential for load bearing applications and for antibacterial coatings. In the investigation developed by N. Marieta et al. [12] nanopowder of Forsterite was fabricated and samples were immersed in SBF for 7 and 28 days. After this period, it was observed by SEM hydroxyapatite formation on the nanopowders.

The activity of the bioceramics is favoured by the presence of porosity. However, porosity imposes a limitation on the mechanical properties of the sample. Porous ceramics, glasses, bioglasses and bioactive crystals are much more fragile than if they were dense. Therefore, a suitable strategy is the use of dense, multiphase ceramics which are capable of generating a certain porosity by dissolving one of the phases in presence of SBF, meeting the mechanical advantages of a dense material and the biological features of a porous scaffold.

In the literature there are a large number of studies related to the degradation of the bioactive phases. However, there is a lack of results related to the behaviour of dense bioceramics containing several bioactive phases, with the exception of the works carried out on the eutectic compositions of the systems based on MgO, CaO, SiO_2 and P_2O_5. M.A. Sainz [13] studied the bioactivity of novel $CaSiO_3$–$CaMg(SiO_3)_2$ bioceramics concluding that the $CaMg(SiO_3)_2$ is significantly less soluble than $CaSiO_3$. Those ceramics were obtained by solid state reaction and sintering unlike the materials studied in this work that have been obtained from the melt.

The purpose of our work is to design a new bioceramic composition in the system CaO–MgO–SiO_2–P_2O_5 that allows the formation of several bioactive phases under different solidification conditions and the study of the evolution of these phases when soaking in SBF. The objective is to obtain information about the dissolution or transformation kinetic of the different phases to control the final porosity and microstructure, adapting it to the different requirements of the bone implant.

2. Materials and methods

2.1. Ceramic powder and precursors preparation

The starting ceramic powders were the following oxides: Magnesium Oxide (MgO, purity: 99.95%, Alfa Aesar, Massachusetts, United States), Silicium Oxide (SiO_2, purity: 99.8%, Alfa Aesar, Haverhill, Massachusetts, United States), Calcium Oxide (CaO, purity: 99.9%, Aldrich, Saint Louis, Missouri, United States), Calcium Silicate ($CaSiO_3$, purity: 99%, Aldrich, Saint Louis, Missouri, United States), Calcium Silicate Phosphate ($Ca_3(PO_4)_2$, purity: 99%, ERBA Pharm, Val de Reuil, Les Andelys, France). The required composition, shown in Table 1, was mixed and homogenized with polyvinyl alcohol in an agate mortar. The mixed powder was cold isostatically pressed at 250 MPa into rods of about 4 mm in diameter and 50 mm long followed by sintering in a furnace at 1200 °C for 12 h. This composition was designed to obtain different coexisting bioactive phases by solidification of the melt.

Table 1
Composition (wt %) of the starting powder.

Compound	% Weight
MgO	13.02
SiO_2	19.43
CaO	18.14
$CaSiO_3$	18.71
$Ca_3(PO_4)_2$	30.70

2.2. Directional solidification of the ceramic rods by the laser floating zone (LFZ) technique

The sintered rods were directionally solidified by the LFZ method. This technique uses a CO_2 laser as heating source (Blade-600, Electronic Engineering). The laser beam is shaped into a ring by mirrors and focused on the precursor forming a small molten zone as a liquid bridge between a seed and the precursor. The zone is moved along the sample at a controlled speed resulting in a directionally solidified rod [14]. The travel speed of the molten zone was controlled varying the speed of the axes where the rods were placed. To improve the heat distribution around the ceramic counter rotation of the upper and lower axis was applied. In order to eliminate the precursor porosity a first densification step was performed. The final growth was carried out moving the molten zone upwards to achieve a solidification front free of bubbles.

The grown speeds selected for this study were 15, 50 and 100 mm/h with 50 rpm counter rotation. As the growth rate has a determinant influence on the microstructure of the samples, phase formation and elemental composition of the phases for all the materials were examined by FE-SEM. The cooling rates were 2, 7 and 14 K/s for growth rates of 15, 50 and 100 mm/h, respectively. The axial temperature gradient at the solid-liquid interface was of the order of 5×10^5 K/m measured with a pyrometer (model Minolta/Land Cyclops 52) covering a range between 600 °C and 3000 °C.

2.3. Microstructural and mechanical characterization

Microstructural characterization was performed in polished transverse and longitudinal cross sections of rods by means of back-scattered electron images obtained in a Field Emission SEM (FESEM, model Carl Zeiss MERLIN). Quantitative analyses of Mg, P, Ca, Si and O were conducted by means of the energy-dispersive X-ray spectroscopy (EDS) detector coupled to the FE-SEM (INCA, 350, Oxford Instruments) at 15 KeV. The digital processing of the images was carried out with the application DigitalMicrograph™. Specimens for this characterization were prepared using conventional metallographic procedures.

Crystalline phase identification was carried out by X-Ray diffraction (XRD). The data were collected with a "D-Max/2500 Rigaku" diffractometer, fitted with a rotating Cu anode. The diffractometer operates at 40Kv and 80 mA and a graphite monochromator is used to select Cu K_α radiation. Measurement conditions of 2theta 5° to 80° step = 0.03 t = 1s/step were chosen.

In order to obtain mechanical properties such as hardness and toughness, micro indentations were performed on the polished surfaces of the unsoaked samples using a diamond Vickers indenter, in the form of a pyramid, on a microhardness tester Matsuzawa, MXT 70. Samples grown at 15, 50, 100 mm/h were tested applying a load of 300 gf during 15 s.

The elastic modulus and hardness values of the sample grown at 15 mm/h were evaluated using nanoindentation technique. These tests were performed with a Berkovich indenter registering in a continuous way and with high precision the load and displacement that experiments the indenter when it penetrates the sample surface. In this essay a charge of 30 gf is applied during 20 iterations.

To calculate toughness the expression given by eq. (1) [15] was used:

$$K_{IC} = 0.015\left(\frac{l}{a}\right)^{-1/2}\left(\frac{E}{H}\right)^{2/3}\frac{P}{c^{3/2}} \quad (1)$$

E is the Elastic Modulus (GPa) obtained by nanoindentation measurements, H is the value of the Vickers hardness (GPa), P load value (N), "a" is the half diagonal length of the Vickers indent, "l" is the average length of the cracks emanating from the corners of the indent and "c" the distance between the centre of the print to the end of the crack. As $l/a \leq 2.5$ the crack profile is of Palmqvist type.

2.4. Bioactivity analysis

The in vitro activity of the directionally solidified rods was performed by immersing discs of different samples in Simulated Body Fluid (SBF) during several periods of time. Discs were about 3 mm in diameter and 1 mm wide. The SBF solution was prepared according to Kokubo's protocol [16]. After soaking time, the discs taken out from SBF were dried at room temperature and analysed by image field emission scanning electron microscopy (FE-SEM). Depending on the activity of the samples different soaking times were chosen.

3. Experimental results

3.1. Microstructural analysis of the directionally solidified rods

In order to describe the influence of the growth rates on the microstructure, representative FE-SEM images of transverse cross sections of the different specimens grown at 15, 50 and 100 mm/h are shown in Fig. 1(a), (b) and (c), respectively. The different phases were analysed by EDS. The elemental composition in atoms, phase assignation and volume percentage are given in Table 2.

For the lowest growth rate of 15 mm/h (Fig. 1(a)), four different phases can be observed: akermanite (labeled A) and tricalcium phosphate (T) as main phases forming entangled structures with monticellite (M) and small quantities of forsterite (F) between them.

Fig. 1(b) shows a SEM transversal cross section of a sample grown at 50 mm/h. In this micrograph four phases can be identified. These phases are compatible with the composition of akermanite (A), monticellite (M), and Nurse'A phase (N). Another phase (labeled F, the darkest one) corresponds to forsterite (Table 2). It is worth noting that the increase in solidification speed supposes a decrease in the amount of akermanite present in the sample and the formation of calcium silicate phosphate instead of calcium phosphate and in a greater quantity.

In the case of the sample grown at 100 mm/h (Fig. 1(c)), only two phases are present: a monticellite matrix (dark phase, M) with dendrites (light phase, N) distributed throughout the sample in a homogeneous way with a composition corresponding to the Nurse's A phase (Table 2), in a ratio of volumes of 42.60% and 57.40%, respectively. No other phases were observed. At this growth rate, the percentage of Nurse's A phase is similar to that of the previous sample grown at 50 mm/h, while the other phase with a composition close to monticellite occupies the rest of the sample.

As the size of phases in the sample growth at 100 mm/h is too small for an accurate identification by EDS, structural characterization by XRD was made, as shown in Fig. 2. Main peaks are characteristic of Nurse's A-phase described by Nurse et al. [17]. Nurse's A-phase has the hcp hexagonal crystal lattice where one-eighth of the cations of the structure are not occupied [18]. It was not possible to assign peaks to the monticellite phase indicating that the samples processed by laser floating zone at 100 mm/h, possess a glass-ceramic structure where crystalline Nurse's A-phase is embedded in an amorphous non-stoichiometric monticellite matrix. In this amorphous phase, due to the high growth rate, the nucleation of crystalline phases does not take place.

General compositions (% at) of the samples growth at different speeds are compared with the general composition of the starting powders in Table 3. There is a good correlation between both compositions, the initial one and those of the samples grown at different speeds. In addition, the compositions of each element calculated from the elemental analysis of the phases by EDS weighted with its mass percentages are indicated in parentheses.

3.2. In vitro activity and degradation

The results corresponding to the activity after 3 days for the samples grown at 15 and 50 mm/h and 1 week for the sample grown at 100 mm/h are presented in Figs. 3–5. The compositions of the samples in the transformed zone in contact with SBF by EDS microanalysis are collected in Table 4.

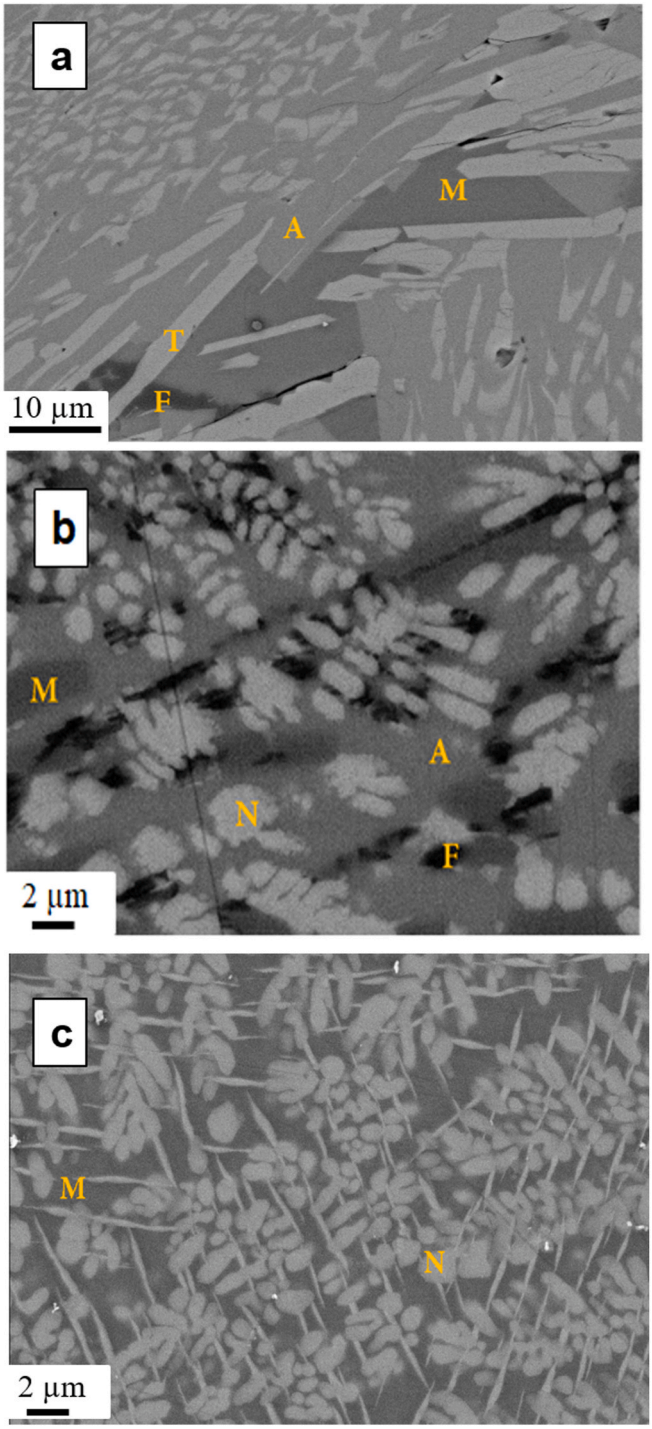

Fig. 1. SEM micrographs of directionally solidified rods grown at: (a) 15 mm/h, (b) 50 mm/h and (c) 100 mm/h. Transverse cross sections.

The affected zone of sample grown at 15 mm/h after SBF soaking period corresponds to the left side of the micrographs shown in Fig. 3(a). This zone is formed by a porous layer of hydroxyapatite (H) resulting from the dissolution of the akermanite phase (phase A in Fig. 1(a)) while the TCP and monticellite phases (phase T and M in Fig. 1(a)), respectively) are transformed to hydroxyapatite, the composition of this porous layer is shown in Table 4. In Fig. 3(b) the transformation of an akermanite/TCP region is shown. Due to the high specific surface of the phases inside the entangled structure of akermanite/TCP, the

Table 2
EDS analysis (atom composition), phase assignation and volume percentage of directional solidified rods grown at 15, 50 and 100 mm/h.

Growth Speed	Phase	O	Mg	Si	P	Ca	Phase name/vol%
15 mm/h	A	6.50	1	2.03	–	2.10	Akermanite ($Ca_2MgSi_2O_7$)/48.46
	M	3.98	1.03	1	–	0.67	Monticellite ($CaMgSiO_4$)/15.24
	F	–	2.1	1	–	–	Forsterite (Mg_2SiO_4)/2,01
	T	8.04	–	–	2	3.10	Tricalcium phosphate $Ca_3((PO)_4)_2$)/34.29
50 mm/h	A	7.45	0.77	2	–	1.92	Akermanite ($Ca_2MgSi_2O_7$)/17.50
	M	4.22	1.21	1.16	–	1	Monticellite ($CaMgSiO_4$)/11.30
	F	4.48	1.66	1	–	–	Forsterite (Mg_2SiO_4)/11.50
	N	15.88	–	2.34	2	6.5	Nurse's A ($Ca_7Si_2P_2O_{16}$)/59.70
100 mm/h	M	4.27	1.24	1.08	–	1	Monticellite ($CaMgSiO_4$)/42,60
	N	16.88	1.64	2.89	2	6.65	Nurse's A ($Ca_7Si_2P_2O_{16}$)/57,40

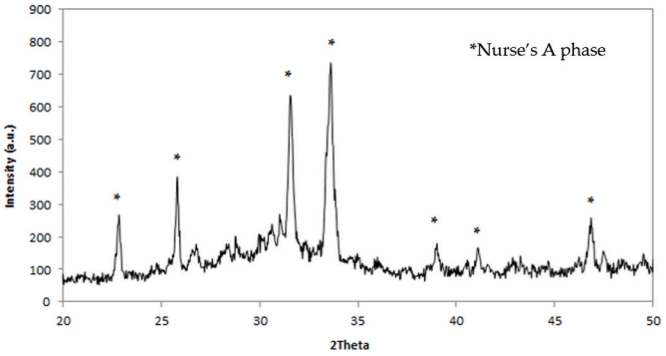

Fig. 2. XRD patterns of the rod samples grown at 100 mm/h.

Table 3
General composition (at %) of the different samples. In parentheses the elemental compositions obtained by EDS of the individual phases weighted by their mass fractions are indicated.

General composition	O	Mg	Si	P	Ca
Starting powder (Table 1)	58.98	7.39	11.09	4.57	17.96
15 mm/h	56.87 (57.7)	8.65 (8.07)	12.39 (11.35)	4.32 (5.08)	17.77 (17.80)
50 mm/h	57.96 (57.60)	8.63 (7.65)	12.08 (12.35)	4.29 (4.32)	17.04 (18.08)
100 mm/h	57.15 (57.08)	7.86 (7.85)	11.87 (11.82)	4.55 (4.77)	18.56 (18.45)

akermanite phase is completely removed, leaving a porous structure of HA as seen in the insert of Fig. 3(b). The deposition of a new apatite phase has not been observed as the magnesium and calcium dissolution in the liquid prevents it. This fact has been observed before by L. Grima et al. [19].

The main phases before the bioactivity test of the ceramic grown at 50 mm/h were akermanite, monticellite and the Nurse's A. After being soaked in SBF for three days, the general trend of the sample is the formation of a layer of hydroxyapatite on the surface (phase H in Fig. 4

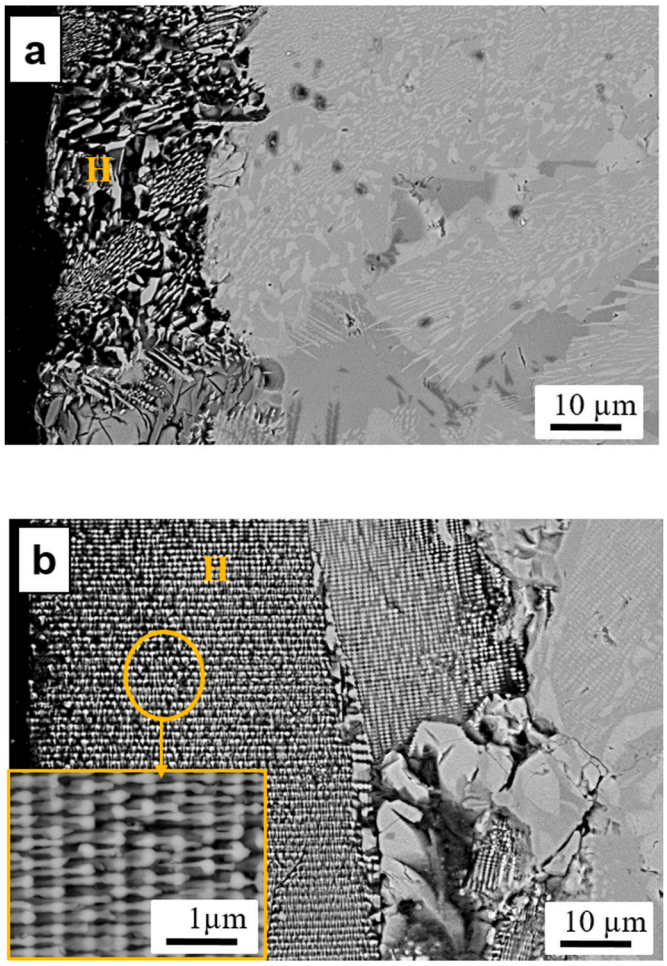

Fig. 3. SEM micrographs of a directionally solidified rod grown at 15 mm/h and after soaking in SBF solution for 3 days: (a) transverse cross section of the rod, (b) transformed Akermanite/TCP región after immersion in SBF in longitudinal cross section. An area with higher magnification is shown in the insert.

(a)), the dissolution of the akermanite phase and the transformation of the monticellite phase into a Ca–P phase (phase CaP in Fig. 4(a)). The dendrites of Nurse's A phase seem to react slower than monticellite, as some of them reached the edge of the sample at this period of time. The dissolution of the akermanite gives to the sample some porosity about 50 µm in depth from the surface in the contact with the fluid.

Unlike the sample grown at 15 mm/h, an apatite layer is deposited on the sample surface by precipitation of calcium ions and phosphorus from the SBF. This may be due to the lower release of active Mg and Ca ions to the liquid since the volume percentage of akermanite formed is lesser at 50 mm/h (17.50%) than at 15 mm/h (48.46%) as indicated in Table 2. In Fig. 4 (b) a longitudinal cross section of the sample surface is shown. In this picture we can analyse the continuity of the phases between the affected and unaffected zones. Meanwhile the akermanite phase dissolves, monticellite and Nurse's A phase starts to transform. The latter does it more slowly since untransformed particles are still visible within the affected area. A HA layer begins to form and apparently the voids left by the dissolved akermanite are filled by HA.

In the case of the sample grown at 100 mm/h, as shown in Fig. 5(a), after 1 week of soaking time a continuous layer of hydroxyapatite is deposited on the surface of the sample. The depth of the affected zone is about 50 µm. Both phases seem to maintain the initial morphology but their composition changes to calcium phosphate phases as indicated in Table 4. The phase with the highest solubility (monticellite) favours the formation of the HA layer on the surface of the sample. Furthermore, the

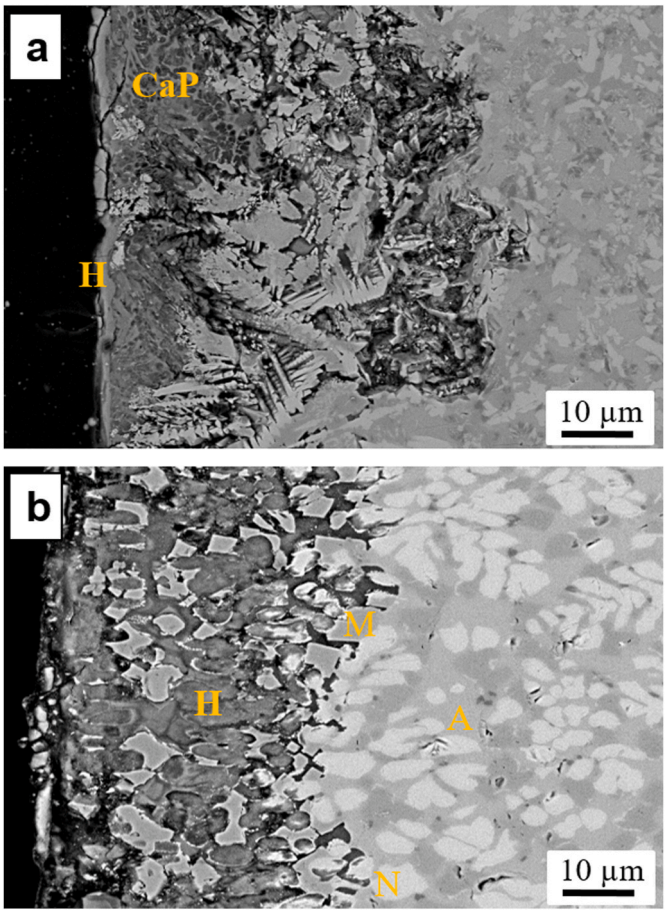

Fig. 4. SEM micrographs of a directionally solidified rod grown at 50 mm/h and after soaking in SBF solution for 3 days: (a) transverse cross section of the rod, (b) longitudinal cross section.

CaP phase provides structural support to the stabilization of the HA layer. In Fig. 5(b) and (c) a longitudinal cross section of the surface sample is shown. Three different zones can be distinguished. The inner zone (right) corresponds to the unaffected part of the sample with a darker phase of monticellite and the Nurse's A phase in form of dendrites. The middle zone corresponds to the area where the monticellite has transformed, faster than dendrites. And in the outer zone, closer to the SBF, both phases have transformed (Fig. 5(b)) while a layer of HA several microns thick covers the surface as shown in Fig. 5(c).

The Ca/P ratio of the HA-layer was 1.68 and 1.72 respectively for the samples grown at 50 and 100 mm/h, very close to that in the HA stoichiometric (1.67).

3.3. Micro hardness and nanoindentation tests

One interesting issue of ceramic scaffolds concerns the mechanical properties before implantation. The micro-hardness and toughness of the samples have been estimated by Vickers indentation. The results are listed in Table 5. According to them, micro-hardness values are close to 4 GPa for all growth rates. It means that the presence of silicate phases like akermanite, monticellite as a matrix with hardness around 4–5 GPa is dominant [20]. Furthermore, phosphate phases like TCP and Nurse's A as reinforcements in the matrix have similar hardness value of 4–4.4 GPa [21]. The only phase with higher hardness is forsterite which can only be something relevant at medium growth rates but did not have strong influence to improve hardness value [22]. So, it can be understood that the hardness values are almost independent of growth rates due to the presence of the same phases with close hardness values.

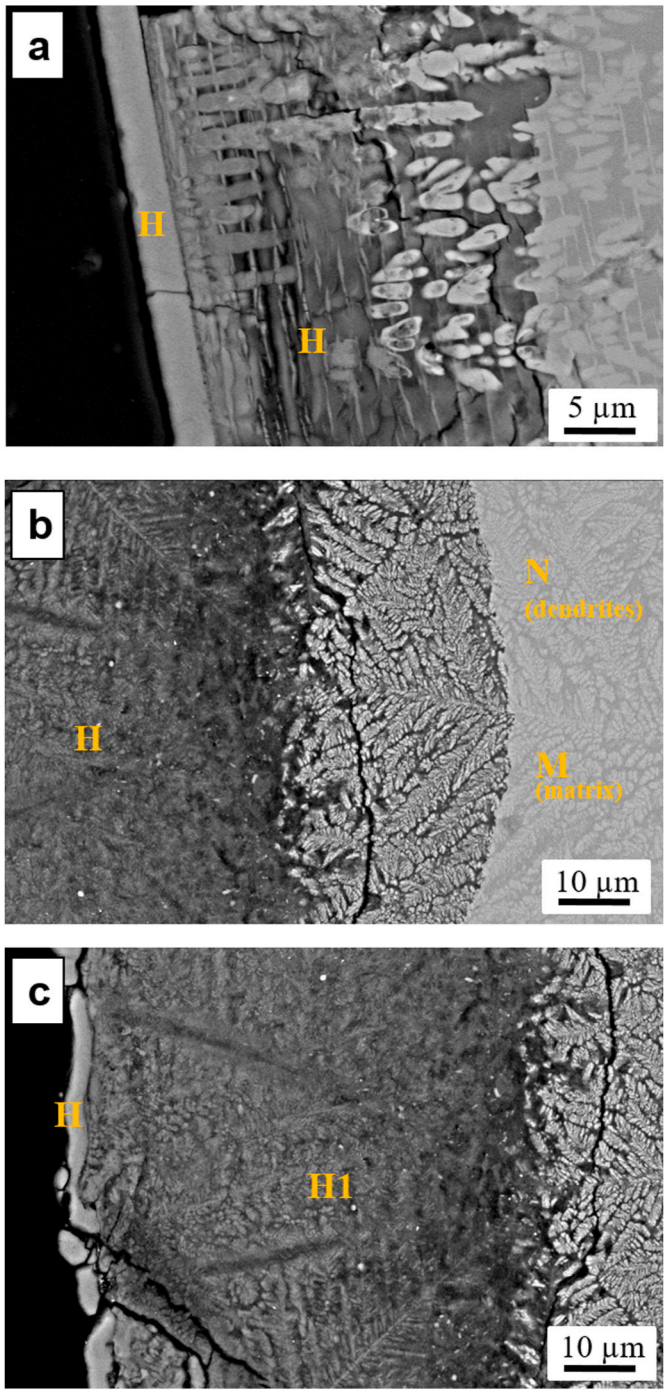

Fig. 5. SEM micrographs of a directionally solidified rod grown at 100 mm/h after soaking in SBF solution for 1 week: (a) transversal cross section (b) longitudinal cross section. Right: unaffected part of the sample, middle: area where the monticellite has transformed and dendrites of Nurse's A phase remain unaltered, left: both phases have transformed to HA (c) longitudinal cross section zone: formation of a HA layer on the surface in contact with SBF.

Fig. 6 shows the typical nanoindentation test loading and unloading curve for a rod grown at 15 mm/h. From this plot it is possible to know the penetration value under maximum load and final penetration value when the indenter stops the contact with the material. This latter value corresponds with plastic deformation of the material after the charge-discharge cycle. As can be observed, the discharge curve does not follow a linear law, since during the removal of the indenter, elastic relaxation leads to a variation of the shape of the footprint and at the

Table 4
EDS analysis (atom composition) for directional solidified rods grown at 15, 50 and 100 mm/h after soaking in SBF solution for different periods of time.

Growth speed	Immersion periods		O	Mg	Si	P	Ca	Ca/P
15 mm/h	Immersed 3 days	H	7.43	0.35	0.06	2	2.79	1.39
50 mm/h	Immersed 3 days	H	4.43	0.12	–	2	3.37	1.68
		CaP	11.90	0.22	0.32	2	2.57	1.28
100 mm/h	Immersed 1 week	H1	4.13	0.11	–	2	3.45	1.72
		H	10.24	0.47	0.30	2	3.12	1.56

Table 5
Vickers hardness and toughness of samples grown at different rates.

Samples (mm/h)	HV (GPa)	K_{IC} (MPa·m$^{1/2}$)
15	5.74 ± 0.88	0.78 ± 0.13
50	4.63 ± 0.27	0.82 ± 0.04
100	4.65 ± 0.49	0.82 ± 0.12

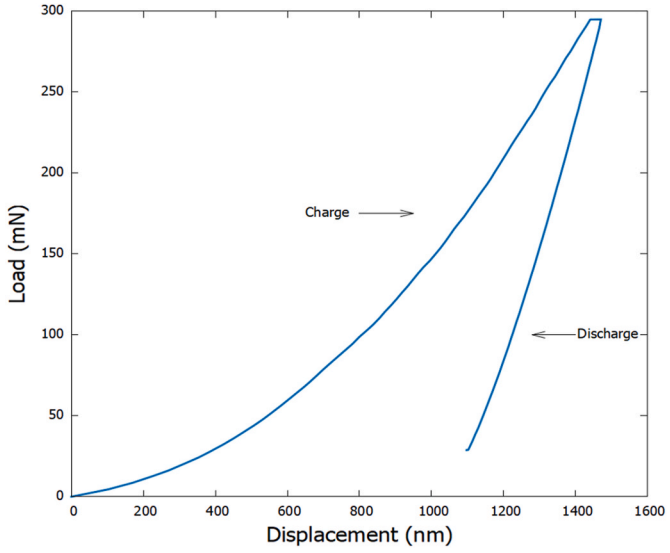

Fig. 6. Indenter load-displacement curves for the rod sample grown at 15 mm/h.

same time of the contact surface. The tests were performed on the sample grown at 15 mm/h because of its better crystallinity. The slope of the unloading curve provides the value of elastic moduli. The hardness was derived by dividing the load by the projected area of contact between the indenter and the specimen. Average values of hardness and elastic modulus obtained with a nanoindentation test during twenty iterations in the sample grown at 15 mm/h are 6.70 ± 1.54 GPa and 122.82 ± 8.67 GPa, respectively. There is a difference between hardness obtained with nanoindentation and Vickers essay in total compliance with nanoindentation theory, whereby hardness value is always dependent on load and contact area of the indenter tip [23]. In the Vickers test a wider contact area was obtained from higher depth of penetration, resulting in lower value of hardness.

The values of hardness and elastic modulus by nanoindentation obtained here are comparatively higher than those values reported by Kumar and Wang for commercial spherical hydroxyapatite [24]. This supports the fact that fabricated ceramic in this study can be useful for load bearing applications.

The toughness values obtained by Vickers tests (Table 5) are comparable to the cortical bone toughness values reported in literature [19]. In general, fracture toughness is found to be essentially grown rates independent. The value of this quantity is ~0.8 MPa m$^{1/2}$. However, a decrease in the value of these properties is expected after immersion in SBF. The partial or total dissolution of some of the phases during immersion, phase transformation or apatite deposition can lead to a mechanical properties degradation as seen by Zysset [25].

4. Discussion

The new ceramic composition studied in this work leads to different microstructures depending on the growth rates. These different microstructures are formed by several bioactive phases that have allowed us to study the rate of degradation and transformation of such phases when they are coexisting in the same material. At 15 mm/h and 50 mm/h growth rates, akermanite is present in the sample as one of the main phases. Monticellite appears in the whole range of growth rates being one of the main phases at a high growth rate. Calcium phosphate phases appear as TCP at low speed and as Nurse's A phase at 15 mm/h and 100 mm/h growth rates. Forsterite, as well as the akermanite, only appears at 15 mm/h and 50 mm/h growth rates as a minor phase. The lower growth rate the higher phase separation takes place, coexisting four different phases, three silicates and one phosphate. By increasing the growth rate, a calcium phosphate silicate is formed instead of calcium phosphate. At higher rates, the Nurse's A phase remains together with an amorphous phase with composition close to that of monticellite.

As a general rule, akermanite dissolves very quickly causing porosity and hindering the formation of a hydroxyapatite layer on the surface of the ceramic in contact with SBF. The other bioactive phases, monticellite, tricalcium phosphate and Nurse's A transform in Ca–P phases but not at the same rate, being Nurse's A phase less active than the others.

The consumption of protons by the rapid magnesium and calcium dissolution (eqs. (2) and (3)) and the deprotonation of silica (eq. (4)) from the akermanite can modify the pH, altering the starting condition and affecting the other phases, for example inhibiting not only the growth, but also the precipitation, of hydroxyapatite crystals on the surface of the sample where TCP is present.

$$MgO\ (s) + 2H^+ \rightarrow Mg^{2+} + H_2O \quad (2)$$

$$CaO\ (s) + 2H^+ \rightarrow Ca^{2+} + H_2O \quad (3)$$

$$SiO_2\ (s) + 2H_2O \rightarrow Si(OH)_4\ (aq) \rightarrow HSiO_4^{3-} + 3H^+ \quad (4)$$

In a first step the Mg–O and Ca–O bonds in silicates break by reaction with H^+ in the solution. The strength of the Mg–O bond is greater than that of Ca–O bond due to its smaller ionic radius, leading to a more difficult dissolution of Mg ions. Subsequently, Si–O on the surface would form an amorphous silica-rich layer negatively charged that would attract dissolved Ca^{2+} from silicates and intrinsic cations in saline solution. This layer is not stable in the sample where akermanite in the active zone is totally dissolved. J. Ma et al. [26] observed that the increase of MgO in sol–gel derived SiO_2–CaO–MgO–P_2O_5 system glasses retarded the formation of apatite layer on glass surface. Vallet-Regi and co-workers also demonstrated that the formation rate of apatite layer slows down when MgO content in the glass is above 7 mol% [27]. These results suggest that a high content of magnesium in solution inhibits bioactivity and can block apatite crystal growth.

The higher dissolution rate of the akermanite with respect to the other phases in our samples is consistent with the results reported by other authors.

Huang et al. [28] studied the dissolution behavior of akermanite, bredigite and diopside powders during soaking in saline solution. Dissolved Ca and Mg ion concentration were proportional to the content of these ions in the chemical compositions.

Strandkvist et al. [29] measured the dissolution of several minerals present in slag, namely dicalcium silicate, pseudowollastonite, monticellite, akermanite and merwinite, by setting the pH to 4, 7 or 10. The

HNO_3 consumption required to maintain the pH level was recorded during 40 h. At neutral pH akermanite dissolved completely after 20 h but monticellite by about 50% at the end of the experiment. Dicalcium silicate reached full dissolution within a few hours. This is coherent with the fact that calcium is more likely to dissolve than magnesium, as can be deduced from Pourbaix diagrams [30]. This fact would also explain the faster dissolution of akermanite with respect to monticellite transformation because of the higher content of magnesium in the latter and supported by the greater number per molecule of active atoms (calcium, magnesium and silicon) in the first.

The Ca, Mg and Si released would be beneficial to accelerate bone tissue regeneration and remodeling. It has been reported that the Mg, Ca and Si ions release from bioceramics for bone regeneration, as akermanite and nagelschmidtite, decreases the immune responses caused by macrophages in vitro and in vivo. This suggests that the alteration of the ionic microenvironment between implant and host may reduce the inflammatory response compared with TCP bioceramic used as a control [31].

Scaffolds composed by two phases (dicalcium silicate and Nurse's A) of different degradation rates for bone tissue engineering have been reported by Navalon et al. [32]. They combined chemical composition, structure and microstructure to achieve an scaffold possessing fast and strong bioactivity. They suggest that at the beginning of the essay in SBF the dicalcium silicate started to dissolve and then two processes occurred at the same: the starting of the Nurse's A phase dissolution and the precipitation of a carbohydroxyapatite layer enhanced by the formation of silanol (Si–OH) groups on the surface.

In our work for the samples where the Nurse's A is present (grown at 50 and above 100 mm/h) a similar behaviour has been seen. The Nurse's A phase experiments a slower transformation and a hydroxyapatite layer covers the surface of the sample in contact with SBF. In these cases, the alkalinization of the medium by the magnesium release can be compensated by the deprotonation of Si while maintaining the appropriate conditions for the HA-like layer nucleation once the Ca and P content exceeds the solubility product of HA. Then, the HA layer grows by reaction of the HPO_4^{2-} ions with the excess of Ca^{2+} ions in the SBF consuming calcium and phosphate ions from the surrounding solution. The formation of an amorphous Si-rich layer prior to HA nucleation can be favoured.

This study describes the successful development of a new bioceramic whose microstructure can be controlled to regulate the release of bioactive ions to the surrounding environment, modulating the dissolution and physico-chemical reactions occurring at the material surface and potentially developing human bone given the well-known role magnesium plays in stimulating osteoblast proliferation. The potential of the new ceramic is to combine bioactivity with mechanical stability or controlled porosity, according to the microstructure chosen by adjusting the growth rate.

5. Conclusions

From the selected ceramic composition and microstructure control through the processing conditions is possible to regulate the response of the material in SBF, being able to obtain a porous scaffold or a bioactive layer according to the properties that the application requires. A porous scaffold may be of interest when bone mechanical properties where it is going to be applied are low. On the other hand, a scaffold without porosity (obtained at high speeds), could be used when bone has major mechanical properties. Porous generation (through akermanite dissolution) has other benefits like calcium and magnesium release to the medium which can be beneficial at the cellular level. The main conclusions can be summarized as follows:

- Crystalline and glass-crystalline rods with composition in the $CaSiO_3$ - $CaMg(SiO_3)_2$ – $Ca_3(PO_4)_2$ system were grown by LFZ. Depending on the growth rate different microstructure and properties are achieved. At 100 mm/h a composite of glass with composition close to that of the monticellite and a crystalline Nurse'A phase is obtained. At an intermediate growth rate of 50 mm/h, phases like monticellite, akermanite and forsterite are also present. At a low speed of 15 mm/h the sample is composed of forsterite, akermanite, monticellite and tricalcium phosphate. All phases are bioactive.
- The in vitro behavior of the samples strongly depends on the microstructure and hence on the processing conditions. Akermite/TCP composites obtained at low growth rates give rise to a porous ceramic of hydroxyapatite by dissolution of the akermanite phase in the SBF and transformation of TCP and monticellite. The leaching of Mg^{2+} ions from sample to solution would reduce the overall rate of calcium phosphate crystallization and delay the transformation of amorphous calcium phosphates to more stable apatite phases preventing the formation of a HA layer in the time studied in this work. This fact could be used to suppress unwanted crystallization in vivo leading to *de novo* tissue development.
- Monticellite/Nurse'A phase composite develops a deposited layer of HAp in the surface and yields a zone with HA composition by simultaneous transformation of both phases supposedly favouring the implant-bone bonding.
- The mechanical properties of the unsoaked samples, elastic modulus (122.82 ± 8.67 GPa), micro-hardness (~4 GPa) and toughness (~0.8 $MPam^{1/2}$) are comparable to other bioceramics used in bone repair and appropriate for load bearing applications.

In summary, by means of solidification parameters control it is possible tailor bioceramics with controlled microstructures and different dissolution behaviour leading either to phase transformation and deposition of a HA layer or to in situ formation of an interconnected porous bioceramic driven by the high solubility of akermanite in SBF. The results in this study provide insight into the response of silico phosphate ceramics and give guidance for future design of bioceramics with controllable ion release for bone engineering applications.

Declaration of competing interest

The authors declare that they have no known competing financial interests or personal relationships that could have appeared to influence the work reported in this paper.

Acknowledgments

The authors would like to acknowledge the use of Servicio General de Apoyo en la Investigación- SAI, Universidad de Zaragoza.

BMM wants to acknowledge the financial support awarded by the Spanish Ministry of Science and Innovation through the grant PID2019-103847RJ-I00, as well as the one provided by the Regional government of the 'Junta de Andalucía' through the project P18-RTJ-1972.

References

[1] V.J. Chen, G. Wei, P.X. Ma, Nanoestructured scaffolds for tissue engineering and regeneration, in: H. Singh Nalwa (Ed.), Handbook of Nanostructured Biomaterials and Their Applications in Nanobiotechnology, 2005, pp. 1–21.
[2] Y. Huang, X. Jin, X. Zhang, H. Sun, J. Tu, T. Tang, J. Chang, K. Dai, In vitro and in vivo evaluation of Akermanite bioceramics for bone regeneration, Biomaterials 30 (28) (2009) 5041–5048.
[3] X. Chen, J. Ou, Y. Kang, Z. Huang, H. Zhu, G. Yin, H. Wen, Synthesis and characteristics of monticellite bioactive ceramic, J. Mater. Sci. Mater. Med. 19 (2008) 1257–1263.
[4] E. Kalantari, S. Morteza Naghib, M.R. Naimi-Jamal, R. Esmaeili, K. Majidzadeh-A, M. Mozafari, Nanostructured monticellite: an emerging player in tissue engineering, Mater. Process. 5 (7) (2018) 15744–15753.
[5] P.N. De Aza, J.I. Peña, Z.B. Luklinska, L. Meseguer-Olmo, Bioeutectic ceramics for biomedical application obtained by laser floating zone method. In vivo Evaluation, Materials (Basel) 7 (4) (2014) 2395–2410, https://doi.org/10.3390/ma7042395.
[6] L. Roseti, V. Parisi, M. Petrea, C. Cavallo, G. Desando, I. Bartoloi, Scaffolds for bone tissue engineering: state of the art and new perspectives, Mater. Sci. Eng. 78 (2017) 1246–1262.

[7] A.J. Salgado, O.P. Coutinho, R.L. Reis, Bone tissue engineering: state of the art and future trends, Macromol. Biosci. 4 (2004) 743–765.
[8] W. Cao, L. Hench, Bioactive materials, Ceram. Int. 22 (1996) 493–507.
[9] R. Rabadan-Ros, P. Mazón, S. Serena, M.A. Sainz, L. Meseguer-Olmo, P.N. De Aza, In vitro behaviour of Nurse's Ass-phase: a new calcium silicophosphate ceramic, J. Eur. Ceram. Soc. 37 (2017) 2943–2952.
[10] M. Kharaziha, M.H. Fathi, Improvement of mechanical properties and biocompatibility of forsterite bioceramic addressed to bone tissue engineering materials, J. Mech. Behav. Biomed. Mater. 3 (7) (2010) 530–537.
[11] J. Vormann, Magnesium: nutrition and metabolism, Mol. Aspect. Med. 24 (1–3) (2003) 27–37, https://doi.org/10.1016/s0098-2997(02)00089-4.
[12] M. Naghiu, M. Gorea, F. Kristály, M. Tomoaia-Cotisel, A new method for synthesis of forsterite nanomaterials for bioimplants, Ceram. Silikaty 58 (4) (2018) 300–307.
[13] M.A. Sainz, P. Pena, S. Serena, A. Caballero, Influence of design on bioactivity of novel $CaSiO_3$-$CaMg(SiO_3)_2$ bioceramics: in vitro simulated body fluid test and thermodynamic simulation, Acta Biomater. 6 (2010) 2797–2807.
[14] I. de Francisco, R.I. Merino, V.M. Orera, A. Larrea, J.I. Peña, Growth of Al_2O_3/$ZrO_2(Y_2O_3)$ eutectic rods by the laser floating zone technique: effect of rotation, J. Eur. Ceram. Soc. 25 (8) (2005) 1341–1350.
[15] K.M. Liang, G. Orange, G. Fantozzi, Evaluation by indentation of fracture toughness of ceramic materials, J. Mater. Sci. Mater. Med. 25 (1990) 207–214.
[16] T. Kokubo, H. Takadama, Simulated Body Fluid (SBF) as a Standard Tool to Test the Bioactivity of Implants, 2008.
[17] R.W. Nurse, J.H. Welch, W. Gutt, High-temperature phase equilibria in the system dicalcium silicate-tricalcium phosphate, J. Chem. Soc. 220 (1959) 1077–1083.
[18] G.J. Lugo, P. Mazón, C. Baudin, P.N. De Aza, "Nurse's A-phase: synthesis and characterization in the binary system Ca_2SiO_4-$Ca_3(PO_4)_2$, J. Am. Ceram. Soc. 98 (10) (2015) 3042–3046.
[19] L. Grima, M. Díaz-Pérez, J. Gil, D. Sola, J.I. Peña, Generation of a porous scaffold with a starting composition in the CaO-SiO_2-MgO-P_2O_5 system in a simulated physiological environment, Appl. Sci. 10 (2020) 312, https://doi.org/10.3390/app10010312.
[20] M. Myat-Htun, H. Mohammadi, A.F. Mohd Noor, M. Kawashita, Y.M. Baba Ismail, Comprehensive investigation of phase formation mechanism and physico-mechanical properties of Ca-Mg-silicate, ASEAN Eng. J. 11 (2021) 37–50.
[21] A. Tricoteaux, E. Rguiti, D. Chicot, L. Boilet, Influence of porosity on te mechanical properties of microporous-TCP bioceramics by usual and instrumented Vickers microindentation, J. Eur. Ceram. Soc. 31 (8) (2011) 1361–1369.
[22] B. Malmal Moshtaghioun, D. Gómez-García, J.I. Peña, Mg_2SiO_4-$MgAl_2O_4$ directionally solidified eutectics: hardness dependence modelled through an array of screw dislocations, J. Eur. Ceram. Soc. 40 (12) (2020) 4171–4176.
[23] R. Lucchini, E. Jiménez Piqué, Nanoindentación de capas de finas de ZrW, 2009. http://hdl.handle.net/2099.1/6726.
[24] R.R. Kumar, M. Wang, Modulus and hardness evaluations of sintered bioceramic powders and functionally graded bioactive composites by nano-indentation technique, Mater. Sci. Eng. 338 (2002) 230–236.
[25] P.K. Zysset, X.E. Guo, C.E. Hoffler, K.E. Moore, S.A. Goldstein, Elastic modulus and hardness of cortical and trabecular bone lamellae measured by nanoindentation in the human femur, J. Biomech. 32 (10) (1999) 1005–1012.
[26] J. Ma, C.Z. Chen, D.G. Wang, Y. Jiao, J.Z. Shi, Effect of magnesia on the degradability and bioactivity of sol-gel derived SiO_2-CaO-MgO-P_2O_5 system glasses, Colloids Surf. B Biointerfaces 81 (1) (2010) 87–95.
[27] A.J. Salinas, J. Román, M. Vallet-Regi, J.M. Oliveira, R.N. Fernandes, In vitro bioactivity of glass and glass-ceramics of the 3CaO.P_2O-CaO.SiO_2-CaO.MgO.2SiO_2 system, Biomaterials 21 (3) (2000) 251–257.
[28] M. Huang, M. Zhang, D. Yao, X. Chen, X. Pu, X. Liao, Z. Huang, G. Yin, Dissolution behavior of CaO-MgO-SiO_2- based bioceramic powders in simulated physiological environments, Ceram. Int. 43 (13) (2017) 9583–9592.
[29] I. Strandkvist, B. Björkman, F. Engström, Synthesis and dissolution of slag minerals-a study of β-dicalcium silicate, pseudowollastonite and monticellite, Can. Metall. Q. 54 (4) (2015) 446–454.
[30] F. Engström, D. Adolfsson, C. Samuelsson, A. Sandström, B. Björkman, A study of the solubility of pure slag minerals, Miner. Eng. 41 (2013) 46–52, https://doi.org/10.1016/j.mineng.2012.10.004.
[31] Y. Huang, W. Chengtie, Z. Xiaoling, J. Chang, D. Kerong, Regulation of immune response by bioactive ions released from silicate bioceramics for bone regeneration, Acta Biomater. 15 (66) (2018) 81–92.
[32] C. Navalón, P. Mazón, P.N. De Aza, "Eutectoid dicalcium silicate-Nurse's A ceramic scaffold: processing and in vitro bioactivity, Ceram. Int. 45 (17) (2019) 21716–21724.